Theoretical description of the electrical double layer for a mixture of n ionic species with arbitrary size and charge asymmetries. I. Spherical geometry

3 authors, including:

Jonathan Josué Elisea Espinoza
Universidad Autónoma de San Luis Potosí
3 PUBLICATIONS   **12** CITATIONS

Guillermo Ivan Guerrero-Garcia
Universidad Autónoma de San Luis Potosí
51 PUBLICATIONS   **787** CITATIONS

Theoretical description of the electrical double layer for a mixture of *n* ionic species with arbitrary size and charge asymmetries. I. Spherical geometry ⊘

Jonathan Josué Elisea-Espinoza (ID) ; Enrique González-Tovar (ID) ; Guillermo Iván Guerrero-García ✉ (ID)

Check for updates

View Online   Export Citation   CrossMark

The Journal of Chemical Physics

AIP Publishing

Theoretical description of the electrical double layer for a mixture of *n* ionic species with arbitrary size and charge asymmetries. I. Spherical geometry

Jonathan Josué Elisea-Espinoza,[1] (ID) Enrique González-Tovar,[1] (ID) and Guillermo Iván Guerrero-García[2,a] (ID)

AFFILIATIONS

[1] Instituto de Física de la Universidad Autónoma de San Luis Potosí, Álvaro Obregón 64, 78000 San Luis Potosí, Mexico

[2] Facultad de Ciencias de la Universidad Autónoma de San Luis Potosí, Av. Chapultepec 1570, Privadas del Pedregal, 78295 San Luis Potosí, Mexico

[a] Author to whom correspondence should be addressed: givan@uaslp.mx

ABSTRACT

In this work, we propose a theoretical finite element description of the ionic profiles of a general mixture of *n* species of spherical charged particles dissolved in an implicit solvent, with arbitrary size and charge asymmetries, neutralizing a spherical macroion. This approach aims to close the gap between the nano- and the micro-scales in macroion solutions, taking into account the ion correlations and ionic excluded volume effects consistently. When these last two features are neglected, the classical non-linear Poisson–Boltzmann theory for *n* ionic species—with different ionic closest approach distances to the colloidal surface—is recovered as a limit case. As a proof of concept, we study the electrical double layer of an electroneutral mixture of oppositely charged colloids and small microions, with an asymmetry 1:333 in size and 1:10 in valence, in salt-free and added salt environments. Our theoretical approach displays a good agreement regarding the ionic profiles, the integrated charge, and the mean electrostatic potential obtained from molecular dynamics simulations with explicit-sized microions. Although the non-linear Poisson–Boltzmann colloid–colloid and colloid–microion profiles differ notably from those obtained via molecular dynamics simulations with explicit small-sized ions, the associated mean electrostatic potential agrees well with the corresponding explicit microion simulations.

Published under an exclusive license by AIP Publishing. https://doi.org/10.1063/5.0151140

I. INTRODUCTION

The ionic cloud surrounding a charged colloidal surface is the so-called electrical double layer. The electrical double layer determines the electrostatic and thermodynamic properties of charged colloidal solutions, e.g., Refs. 1–3. In these systems, colloidal particles can have diameters of the order of microns, whereas small counterions have ionic diameters of a few angstroms. As a result, high size and charge asymmetries are typically present in the solutions of charged colloids, or macroions, dissolved in supporting aqueous electrolytes.

In molecular simulations, the study of charged fluids requires considering a huge number of particles if solvent molecules are taken into account explicitly. This approach has the advantage of including specific interactions and atomistic details present in real or experimental systems. Nevertheless, when large asymmetries in charge, size, and/or concentration among different species are present, the number of particles that must be considered in a simulation box can be prohibitively large and expensive, from a computational point of view. For this reason, coarse-grained approaches such as the so-called primitive model have been proposed in the past to characterize charged fluids, e.g., Refs. 4–6. In this description, the ionic species are modeled as spherical repulsive-core particles with point charges embedded in their centers, which are dissolved in a continuous solvent. Despite its simplicity, the primitive model has been shown to be able to include relevant characteristics of Coulombic fluids, such as ion correlations or ionic excluded volume effects. When these features are included consistently in computer

TABLE I. Some studies of nanoparticle solutions in implicit solvents where ion correlations and ionic excluded volume effects are taken into account considering small ions explicitly, via theory and/or simulation. Note that DLVO-Yukawa-like theories were excluded.

Year	Max. species	Max. size ratio	Max. valence ratio	Kind of study	Reference
1982	4	125/1	120/1	Theory	40
1998	2	7.5/1	20/1	Simulation	41
1999	2	10/1	60/1	Simulation	42
2000	2	200/1	80/1	Simulation	43
2005	4	20/2	22/1	Simulation	44
2011	3	7.06/1	54/1	Theory and simulation	27
2013	3	17/1	54/1	Theory and simulation	45
2014	4	1322.75/1	750/1	Theory and simulation	28
2015	3	250/1	80/1	Simulation	34
2018	3	10/1	106.25/1	Theory and simulation	32
2020	2	10/1	12/2	Theory and simulation	29
2022	3	600/1	200/1	Simulation	38
2022	3	600/1	100/1	Simulation	39
2023	6	333/1	10/1	Theory and simulation	This work

simulations or theoretical approaches, interesting experimental phenomena such as charge inversion, charge reversal, and surface charge amplification arise, e.g., Refs. 4–11.

From a theoretical perspective, many frameworks have been proposed to mimic the electrical double layer in the primitive model, which takes into account ion correlations and ionic volume effects. Some of these approaches include classical density functional theories,[12–25] the modified Poisson–Boltzmann equation,[26] or integral equations theories based on the Ornstein–Zernike equation.[27–29] In the latter, a closure is needed to be able to calculate the ionic profiles of the charged species consistently. In this regard, one of the most successful approaches is the one based on the hypernetted-chain closure.[30] In the classical formulation of this scheme, an equally sized grid has been used to calculate the Fourier transforms that allow us to solve numerically the Ornstein–Zernike equation, which makes it very difficult to consider large size asymmetries between a pair of ionic species from a computational perspective. This limitation has been overcome by Heinen *et al.* by using Fourier transforms with logarithmically spaced grids in n dimensions.[28] As a result, they have been able to study colloidal systems with three and four components, maximum size asymmetries 1322.75:1, and maximum charge asymmetries 750:1. In that study, they have observed a good agreement between their theoretical hypernetted-chain (HNC) calculations and molecular dynamics simulations with up to 28 080 particles in 1:1 supporting electrolytes. On the other hand, as an alternative to the fully consistent application of the HNC closure to the Ornstein–Zernike equation, the hybrid hypernetted-chain/mean spherical approximation (HNC/MSA) closure has been proposed in the past.[31] This theoretical scheme has allowed us, for example, to study colloidal solutions with the following three components: one species of equally sized macroions dissolved in a binary 1:1 electrolyte with the same ionic radii.[32] In such a paper, maximum size and charge asymmetries 10:1 and 106.25:1, respectively, were studied theoretically using the HNC/MSA approach. In addition, a good agreement was observed between the HNC/MSA data and Monte Carlo simulations for a size

asymmetry 10:1 and charge asymmetries 4:1 and 18:1 at a volume fraction 0.24. Other authors have studied large size and charge asymmetries using contracted or effective theoretical descriptions[33–37] or primitive model molecular simulations in which small counterions are included explicitly.[34,38,39] Despite these efforts, the literature on highly asymmetric colloid-microion solutions is rather scarce due, in part, to the computational cost and numerical limitations mentioned above. To illustrate this, Table I includes diverse theoretical and simulation papers, and it compares the maximum number of species, as well as the maximum size and valence ratio of different nanoparticle solutions considered therein, where ion correlations and ionic excluded volume effects are taken into account by including small sized ions explicitly dissolved in a continuous solvent. Note that DLVO-Yukawa-like theories were excluded in Table I.[27–29,32,34,38–45]

Thus, in this work, we present the explicit kernels associated with the Ornstein–Zernike equation for a general mixture of n species of spherical charged particles, with arbitrary size and charge asymmetries, neutralizing a spherical macroion in the primitive model via the hybrid HNC/MSA closure. In addition, we apply the finite element method to have a set of equations that can be solved numerically via an efficient Newton-Raphson scheme. To validate our theoretical proposal, we have performed molecular dynamics simulations of salt-free and added salt colloidal solutions with four and six charged species, respectively, and size asymmetry 333:1 and charge asymmetry 10:1. Numerical data obtained from the nonlinear Poisson–Boltzmann theory of point ions are also included to highlight the relevance of ion correlations and ionic excluded volume effects in highly asymmetric electrical double layers.

II. MODEL SYSTEM

Let us consider a mixture of n ionic species dissolved in a continuum solvent. In the primitive model, particles are modeled as hard spheres with point charges embedded in their centers. As a particular case, we will numerically solve here a mixture of up to six charged species: two species of equally sized colloidal particles,

TABLE II. Parameters of the systems simulated in this work using molecular dynamics. In the salt-free with neutral macroions (SF–N), four species of repulsive-core spheres (4S-RCS), and salt-free (SF) cases, the total number of particle species is 4. In the added salt (AS) case, the total number of particle species is 6. The temperature and the dielectric constant, ε_r, in the whole space are 298 K and 78.5, respectively.

Case	z_1	z_2	z_3	z_4	z_5	z_6	R_1 (Å)	R_2 (Å)	R_3 (Å)	R_4 (Å)	R_5 (Å)	R_6 (Å)
SF-N	0	0	−1	1	⋯	⋯	1000	1000	3	3	⋯	⋯
4S-RCS	0	0	0	0	⋯	⋯	1000	1000	3	3	⋯	⋯
SF	10	−10	−1	1	⋯	⋯	1000	1000	3	3	⋯	⋯
AS	10	−10	−1	1	−1	1	1000	1000	3	3	5	5

two species of equally sized small ions that are counterions of the colloidal particles, and two species of equally sized small ions corresponding to the added salt. Nevertheless, notice that our general theoretical framework applies to a mixture of n species. The bulk properties of the salt-free (SF) and the added salt (AS) cases are displayed in Table II. The smallest ionic species of diameter 3 Å represent OH^- and H_3O^+ ions, and the ionic species of diameter 5 Å mimic a fully dissociated NaCl electrolyte. A maximum size asymmetry 1:333 and a charge asymmetry 1:10 are considered in such a scenario. Although it is possible to study larger asymmetries in valence, it is worth mentioning that opposite charged colloidal particles can easily percolate due to the Coulombic interactions, forming colloidal gels and even solid clusters at very large colloidal valences. For this reason, we have decided to study the weakly charged regime in the present study. According to Table III, the whole system is electroneutral. For the theoretical calculations, the interaction potential between two particles of species i and j can be written as

$$U_{ij}(r) = \begin{cases} \infty & \text{if } r < \dfrac{R_i + R_j}{2} \\ \dfrac{z_i z_j e_0^2}{4\pi\varepsilon_0\varepsilon_r r} & \text{if } r \geq \dfrac{R_i + R_j}{2} \end{cases} \qquad (1)$$

where R_i and z_i are the diameter and valence of the particle i, $r = |\vec{r}_i - \vec{r}_j|$, e_0 is the proton charge, ε_0 is the vacuum permittivity, and ε_r is the dielectric constant of the solvent.

Given the large number of ions involved in the added salt case, parallel molecular dynamics simulations have been performed. The long-ranged electrostatic interaction between a pair of particles of species i and j can be written as

$$u_{ij}^{el}(r) = \frac{z_i z_j e_0^2}{4\pi\varepsilon_0\varepsilon_r r}, \qquad (2)$$

whereas the corresponding short-ranged repulsive-core potential between a pair of particles i and j, used only in the molecular dynamics simulations, can be written as

$$\beta u_{ij}^{rc}(r) \begin{cases} \infty & \text{if } r \leq \Delta_{ij} \\ 4\left[\left(\dfrac{\sigma_{rc}}{r - \Delta_{ij}}\right)^{12} - \left(\dfrac{\sigma_{rc}}{r - \Delta_{ij}}\right)^6\right] + 1 & \text{if } \Delta_{ij} < r < \Delta_{ij} + 2^{1/6}\sigma_{rc} \\ 0 & \text{if } r \geq \Delta_{ij} + 2^{1/6}\sigma_{rc} \end{cases}$$

$$(3)$$

where $r = |\vec{r}_i - \vec{r}_j|$, $\beta = (k_B T)^{-1}$, T is the temperature of the system, and $\Delta_{ij} = (R_i/2) + (R_j/2) - \sigma_{rc}$. Note that in the definition of the parameter Δ_{ij} used in Eq. (3), $R_i/2$ and $R_j/2$ are the hard sphere radii of species i and j, respectively, and σ_{rc} is a parameter determining the "hardness" of the particles. The repulsive-core potential given by Eq. (3) is a variation of the Weeks-Chandler-Andersen (WCA) potential proposed in 1971.[46] In Eq. (3), the location of the infinite value displayed by the WCA potential is shifted from the origin to the distance $\Delta_{ij} = (R_i/2) + (R_j/2) - \sigma_{rc}$. In the repulsive-core interaction described by Eq. (3), particles can be considered as hard spheres plus a short-ranged and very-steep WCA potential, whose extension is determined by the value of σ_{rc}. Notice that the original WCA potential corresponds to the repulsive part of a shifted Lennard-Jones potential.[46] Moreover, note that

TABLE III. Number of particles N_i and the corresponding molar concentrations c_i associated with the systems simulated in this work using molecular dynamics. In the salt-free with neutral colloids (SF–N), four species repulsive-core spheres (4S-RCS), and the salt-free (SF) systems, the total number of particle species is 4, whereas in the added salt (AS) case, the total number of particle species is 6. In both instances, the length of the cubic simulation box is $L = 10\,000$ Å. By electroneutrality, $N_2 = N_1$, $N_4 = N_3$, and $N_6 = N_5$. Notice that as the number and the size asymmetry of the particles in the SF-N, 4S-RCS, and SF systems are the same, they have the same volume fraction. These three systems differ only in the valences of the particle species as shown in Table II. Moreover, note that the added salt concentration is 100 times the concentration of the colloidal particles. $\kappa_D = 1/\lambda_D$, where λ_D is the Debye length of the corresponding system.[1–3]

Case	N_1	N_3	N_5	$c_1 (M)$	$c_3 (M)$	$c_5 (M)$	Particles	κ_D (Å^{-1})	λ_D (Å)	Vol. frac.
SF-N	120	1200	⋯	2×10^{-7}	2×10^{-6}	⋯	2 640	4.65×10^{-4}	2150.52	0.126 124 5
4S-RCS	120	1200	⋯	2×10^{-7}	2×10^{-6}	⋯	2 640	0	⋯	0.126 124 5
SF	120	1200	⋯	2×10^{-7}	2×10^{-6}	⋯	2 640	1.54×10^{-3}	648.41	0.126 124 5
AS	120	1200	12 044	2×10^{-7}	2×10^{-6}	2×10^{-5}	26 728	2.13×10^{-3}	469.28	0.126 126 1

in the limit in which the "hardness" parameter σ_{rc} goes to 0, the repulsive-core interaction potential defined in Eq. (3) reduces to the hard spheres potential defined in Eq. (1) (with $z_i = z_j = 0$) for the diameters R_i and R_j used in the definition of Δ_{ij}. The interaction potentials colloid–colloid, colloid–ion, and ion–ion corresponding to Eqs. (2) and (3), used in the MD simulations performed in this work, are plotted in the supplementary material. In addition, the colloid–colloid DLVO interaction potential using the Debye length associated with the salt-free (SF) and the added salt (AS) systems (defined in Table III) is also compared with the bare Coulomb potential in the supplementary material.

III. MOLECULAR DYNAMICS SIMULATIONS

Simulations of charged particles with interacting potentials given by Eqs. (2) and (3) have been performed in the NVT ensemble with $\sigma_{rc} = 1$ Å using a Nosé–Hoover thermostat. The HOOMD-Blue package[47,48] with the Particle–Particle Particle–Mesh (PPPM) methodology[49] compiled with double precision was employed to take into account properly the long-range electrostatic interactions. The specific parameters used in the PPPM were chosen using the methodology proposed by Deserno and Holm[50] to have an RMS error smaller than 1×10^{-6}. After minimizing the total energy of a random configuration, an initial time step of 1×10^{-8} (in reduced units[47]) has been used to start the thermalization process. The initial time step is then periodically increased until a value of 1×10^{-3} (in reduced units[47]) is reached eventually. At this point, at least 2000×10^6 time steps were used to thermalize the system. The position of all particles was sampled for each 1×10^5 MD time steps (in a compromise between efficiency and reduction of time correlations) and at least $20\,000 \times 10^6$ time steps were performed to calculate the time averages. The numerical calculations were performed in an A100 Nvidia GPU installed in a Supermicro server SYS-740P-TRT with 2 Intel Xeon 3rd Gen Scalable Gold 5320 processors. Molecular dynamics simulations for similar colloidal size-asymmetric systems have been reported recently.[34,38,39]

IV. INTEGRAL EQUATIONS THEORY FOR A MIXTURE OF n IONIC SPECIES

The Ornstein–Zernike equations describing the ionic cloud of n species of charged particles around a single spherical macroion of valence z_M and diameter R_M can be written as

$$h_{Mj}(r) = c_{Mj}(r) + \sum_{\ell=1}^{n} \rho_\ell^{bulk} \int h_{M\ell}(t) c_{\ell j}(|\vec{r} - \vec{t}|) dV, \quad (4)$$

where $h_{Mj}(r) = g_{Mj}(r) - 1$ are the total ionic correlation functions, $g_{Mj}(r)$ are the ionic radial distribution functions, and ρ_ℓ^{bulk} are the bulk number densities per unit volume of the particle species. A representation of the macroion in spherical coordinates is given in Fig. 1. The direct correlation functions between ions and the spherical colloid are specified by using the hypernetted-chain (HNC) closure $c_{Mj}(r) = -\beta U_{Mj}(r) + h_{Mj}(r) - \ln[h_{Mj}(r) + 1]$. If $c_{\ell j}(|\vec{r} - \vec{t}|) = -\beta(z_\ell z_j e_0^2)/(4\pi\varepsilon_0\varepsilon_r|\vec{r} - \vec{t}|)$ are employed in the right-hand side of Eq. (4), the integral equations version of the non-linear Poisson–Boltzmann theory is then obtained.[51,52] If $c_{\ell j}(|\vec{r} - \vec{t}|)$
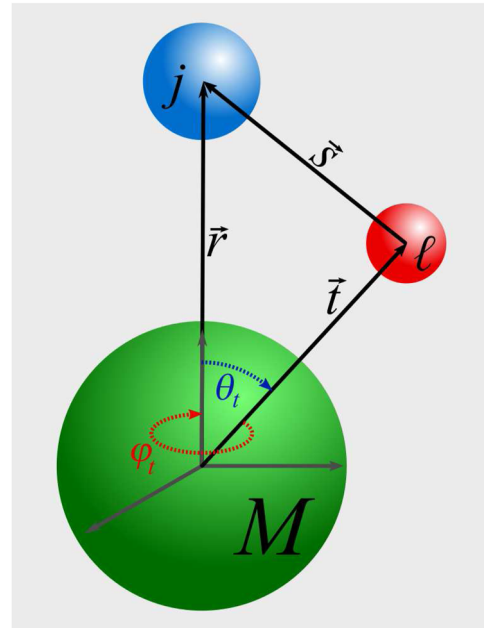
FIG. 1. Schematic representation of the model system used in the theoretical description of the electrical double layer in spherical coordinates. A central macroparticle M is placed at the origin, and ions of species j and ℓ are located at the positions $\vec{r}$ and $\vec{t}$, respectively. The separation distance between the ions of species j and ℓ is $s = |\vec{s}| = |\vec{r} - \vec{t}|$. The convolution integrals in the Ornstein–Zernike equation [Eq. (4)] are performed in the whole space considering a polar angle θ_t and an azimuthal angle φ_t.

are approximated by the bulk direct correlation functions obtained from the mean spherical approximation (MSA), then the HNC/MSA integral equation theory is obtained

$$g_{Mj}(r) = \exp\left[-\beta U_{Mj}(r) + H_{Mj}(r) - K_{Mj}\right], \quad (5)$$

with

$$H_{Mj}(r) = \sum_{\ell=1}^{n} \rho_\ell^{bulk} \int g_{M\ell}(t) c_{\ell j}^{MSA}(s) dV, \quad (6)$$

$$K_{Mj} = \sum_{\ell=1}^{n} \rho_\ell^{bulk} \int c_{\ell j}^{MSA}(s) dV, \quad (7)$$

and $s = |\vec{r} - \vec{t}|$. The MSA direct correlation functions can be written as the sum of an electrostatic and a hard sphere contribution,

$$c_{\ell j}^{MSA}(s) = c_{\ell j}^{hs}(s) + c_{\ell j}^{elec}(s). \quad (8)$$

If the average of the sum and difference of the ionic diameters of species i and j are defined as $R_{ij} = (R_j + R_i)/2$ and $\lambda_{ij} = (R_j - R_i)/2$, respectively, the MSA direct correlation functions can be written in terms of $s = |\vec{r} - \vec{t}| = \sqrt{r^2 + t^2 - 2rt \cos\theta}$ as it is shown in Appendix A.

To obtain the specific kernels of the Ornstein–Zernike equation for the HNC/MSA approach, the three-dimensional space is considered a collection of points $\vec{t} = (t, \theta, \varphi)$, and it is partitioned as follows (see the graphical representation in Fig. 2):

$$\Omega(\vec{t}) = \Omega_{M\ell}(\vec{t}) \ \cup \ \left(\bigcup_{u=1}^{3} \bigcup_{o=1}^{u} \bigcup_{m \in \{A,B\}} \Omega_{\ell j}^{uom}(\vec{t}) \right), \qquad (9)$$

with

$$
\begin{aligned}
\Omega_{M\ell}(\vec{t}) &= \{ \vec{t} = (t, \theta, \varphi) \ : \ 0 \le t < R_{M\ell}, \quad |r-t| \le s \le (r+t) \}, \\
\Omega_{\ell j}^{11A}(\vec{t}) &= \{ \vec{t} = (t, \theta, \varphi) \ : \ R_{M\ell} \le t < r - R_{\ell j}, \quad |r-t| \le s \le (r+t) \}, \\
\Omega_{\ell j}^{21A}(\vec{t}) &= \{ \vec{t} = (t, \theta, \varphi) \ : \ r - R_{\ell j} \le t < r - \lambda_{\ell j}, \quad R_{\ell j} \le s \le (r+t) \}, \\
\Omega_{\ell j}^{22A}(\vec{t}) &= \{ \vec{t} = (t, \theta, \varphi) \ : \ r - R_{\ell j} \le t < r - \lambda_{\ell j}, \quad |r-t| \le s < R_{\ell j} \}, \\
\Omega_{\ell j}^{31A}(\vec{t}) &= \{ \vec{t} = (t, \theta, \varphi) \ : \ r - \lambda_{\ell j} \le t < r, \quad R_{\ell j} \le s \le (r+t) \}, \\
\Omega_{\ell j}^{32A}(\vec{t}) &= \{ \vec{t} = (t, \theta, \varphi) \ : \ r - \lambda_{\ell j} \le t < r, \quad \lambda_{\ell j} \le s < R_{\ell j} \}, \\
\Omega_{\ell j}^{33A}(\vec{t}) &= \{ \vec{t} = (t, \theta, \varphi) \ : \ r - \lambda_{\ell j} \le t < r, \quad |r-t| \le s < \lambda_{\ell j} \}, \\
\Omega_{\ell j}^{31B}(\vec{t}) &= \{ \vec{t} = (t, \theta, \varphi) \ : \ r \le t < r + \lambda_{\ell j}, \quad R_{\ell j} \le s \le (r+t) \}, \\
\Omega_{\ell j}^{32B}(\vec{t}) &= \{ \vec{t} = (t, \theta, \varphi) \ : \ r \le t < r + \lambda_{\ell j}, \quad \lambda_{\ell j} \le s < R_{\ell j} \}, \\
\Omega_{\ell j}^{33B}(\vec{t}) &= \{ \vec{t} = (t, \theta, \varphi) \ : \ r \le t < r + \lambda_{\ell j}, \quad |r-t| \le s < \lambda_{\ell j} \}, \\
\Omega_{\ell j}^{21B}(\vec{t}) &= \{ \vec{t} = (t, \theta, \varphi) \ : \ r + \lambda_{\ell j} \le t < r + R_{\ell j}, \quad R_{\ell j} \le s \le (r+t) \}, \\
\Omega_{\ell j}^{22B}(\vec{t}) &= \{ \vec{t} = (t, \theta, \varphi) \ : \ r + \lambda_{\ell j} \le t < r + R_{\ell j}, \quad |r-t| \le s < R_{\ell j} \}, \\
\Omega_{\ell j}^{11B}(\vec{t}) &= \{ \vec{t} = (t, \theta, \varphi) \ : \ r + R_{\ell j} \le t < \infty, \quad |r-t| \le s \le (r+t) \},
\end{aligned}
$$
(10)

where θ belongs to the interval $[0, \pi]$ and φ belongs to the interval $[0, 2\pi]$ in spherical coordinates (see Fig. 1).

Given that the MSA direct correlation functions are known analytically, it is possible to perform the angular integrals using the partition of the three-dimensional space given above. As a result, it is possible to write Eqs. (6) and (7) as

$$
H_{Mj}(r) = \sum_{\ell=1}^{n} \rho_\ell^{bulk} \sum_{u=1}^{3} \sum_{o=1}^{u} \sum_{m \in \{A,B\}} \sum_{v=1}^{5}
$$

$$
\int_{\mathrm{P}_{\ell j}^{*(u,m)}}^{\mathrm{Q}_{\ell j}^{*(u,m)}} g_{M\ell}(t) \, \vartheta_{\ell j}(o,v) \, \mathcal{J}\left(v, \check{\Lambda}_{\ell j}^{(u,o)}, \, \hat{\Lambda}_{\ell j}^{(u,o)}, r, t \right) dt,
$$
(11)

$$
K_{Mj} = \sum_{\ell=1}^{n} \rho_\ell^{bulk} \sum_{u=1}^{3} \sum_{v=1}^{5} \vartheta_{\ell j}(u,v) \ \mathcal{F}\left(v, \dot{\Lambda}_{\ell j}^{(u)}, \ddot{\Lambda}_{\ell j}^{(u)} \right), \qquad (12)
$$

where

$$
\mathcal{J}\left(v, \check{\Lambda}_{\ell j}^{(u,o)}, \hat{\Lambda}_{\ell j}^{(u,o)}, r, t \right) = \frac{2\pi t}{v \, r} \left[\left[\hat{\Lambda}_{\ell j}^{(u,o)} \right]^{v} - \left[\check{\Lambda}_{\ell j}^{(u,o)} \right]^{v} \right], \qquad (13)
$$
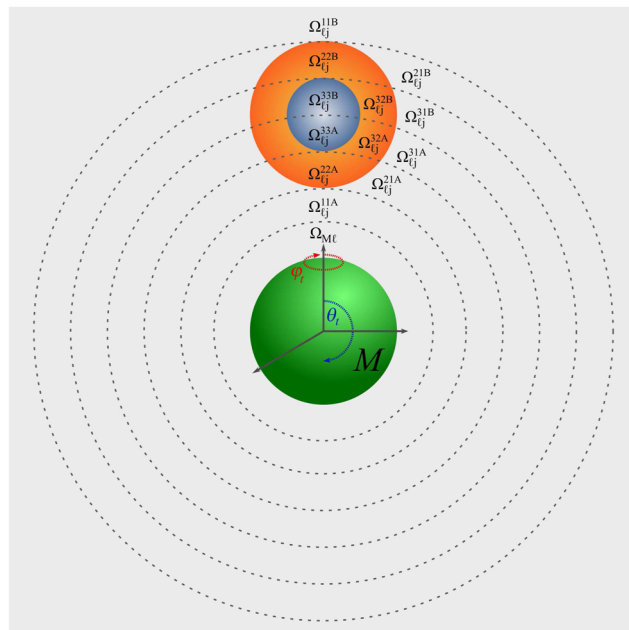
FIG. 2. Schematic representation of the spatial partition of the three-dimensional space used to integrate the Ornstein–Zernike equation [Eq. (4)]. The $\Omega_{\ell j}^{uom}(\vec{t})$ regions used in the convolution integrals are represented explicitly. The blue and orange regions represent the overlapping regions between two particles of species j and ℓ where the hard-sphere contributions of the MSA direct correlation functions are non-zero. In the NLPB theory, the radius of the blue and orange regions is equal to zero. The convolution integrals in Eq. (4) are performed in the whole space using this spatial partition considering a polar angle θ_t and an azimuthal angle φ_t.

$$
\mathcal{F}\left(v, \dot{\Lambda}_{\ell j}^{(u)}, \, \ddot{\Lambda}_{\ell j}^{(u)} \right) = \frac{4\pi}{v+1} \left[\left[\ddot{\Lambda}_{\ell j}^{(u)} \right]^{v+1} - \left[\dot{\Lambda}_{\ell j}^{(u)} \right]^{v+1} \right], \qquad (14)
$$

$$
\check{\mathbf{\Lambda}}_{\boldsymbol{\ell j}} =
\begin{bmatrix}
|r-t| & 0 & 0 \\
R_{\ell j} & |r-t| & 0 \\
R_{\ell j} & \lambda_{\ell j} & |r-t|
\end{bmatrix}, \qquad (15)
$$

$$
\hat{\mathbf{\Lambda}}_{\boldsymbol{\ell j}} =
\begin{bmatrix}
(r+t) & 0 & 0 \\
(r+t) & R_{\ell j} & 0 \\
(r+t) & R_{\ell j} & \lambda_{\ell j}
\end{bmatrix}, \qquad (16)
$$

$$
\dot{\mathbf{\Lambda}}_{\boldsymbol{\ell j}} =
\begin{bmatrix} R_{\ell j} & \lambda_{\ell j} & 0 \end{bmatrix}^{T}, \qquad (17)
$$

$$
\ddot{\mathbf{\Lambda}}_{\boldsymbol{\ell j}} =
\begin{bmatrix} t_{max} & R_{\ell j} & \lambda_{\ell j} \end{bmatrix}^{T}, \qquad (18)
$$

$$\mathbf{P}_{\ell j} = 2 \begin{array}{c} \\ 1 \\ \\ 2 \\ \\ 3 \end{array} \begin{array}{cc} A & B \\ \left[\begin{array}{cc} R_{M\ell} & r + R_{\ell j} \\ \\ r - R_{\ell j} & r + \lambda_{\ell j} \\ \\ r - \lambda_{\ell j} & r \end{array} \right], \end{array} \tag{19}$$

$$\mathbb{Q}_{\ell j} = 2 \begin{array}{c} \\ 1 \\ \\ 2 \\ \\ 3 \end{array} \begin{array}{cc} A & B \\ \left[\begin{array}{cc} r - R_{\ell j} & t_{max} \\ \\ r - \lambda_{\ell j} & r + R_{\ell j} \\ \\ r & r + \lambda_{\ell j} \end{array} \right], \end{array} \tag{20}$$

$$\mathrm{P}_{\ell j}^{*(u,m)} = \max\left(\mathrm{P}_{\ell j}^{(u,m)}, \ R_{M\ell} \right), \tag{21}$$

$$\mathbb{Q}_{\ell j}^{*(u,m)} = \max\left(\mathbb{Q}_{\ell j}^{(u,m)}, \ R_{M\ell} \right), \tag{22}$$

with t_{max} being the upper limit of the integrals corresponding to Eqs. (18) and (20) when it goes to infinity, and the superindex T indicates the transpose operation over the vector to which it has been applied. The matrix $\vartheta_{\ell j}(u, v)$ is defined in Appendix B.

To solve Eq. (5) via the finite element method, we approximate the radial distribution between the ionic species j and the central macroion M by a linear combination of a set of linearly independent basis functions $\phi_i(r)$

$$g_{Mj}(r) \approx \widetilde{g}_{Mj}(r) = \sum_{i=1}^{N_j} \gamma_{Mji} \, \phi_i(r), \tag{23}$$

where γ_{Mji} are the real coefficients and N_j indicates the maximum number of nodes for the species j. In this work, we have used second-order Lagrange interpolating polynomials, which have associated a good equilibrium between algorithmic complexity and computational cost.[53]

By substituting $\widetilde{g}_{Mj}(r)$ in Eq. (5) and $\widetilde{g}_{M\ell}(r)$ in Eq. (11), we obtain

$$\widetilde{g}_{Mj}(r) = \sum_{i=1}^{N_j} \gamma_{Mji} \, \phi_i(r) = \exp\left[-\beta U_{Mj}(r) + \widetilde{H}_{Mj}(r; \vec{\gamma}) - K_{Mj} \right], \tag{24}$$

and

$$\widetilde{H}_{Mj}(r; \vec{\gamma}) = \sum_{\ell=1}^{n} \sum_{u=1}^{3} \sum_{o=1}^{u} \sum_{m \in \{A,B\}} \sum_{v=1}^{5} \rho_\ell^{bulk} \int_{\mathrm{P}_{\ell j}^{*(u,m)}}^{\mathbb{Q}_{\ell j}^{*(u,m)}}$$
$$\left[\left(\sum_{d=1}^{N_\ell} \gamma_{M\ell d} \, \phi_d(t) \right) \vartheta_{\ell j}(o, v) \times \right. \tag{25}$$
$$\left. \mathcal{J}(v, \check{\Lambda}_{\ell j}^{(u,o)}, \hat{\Lambda}_{\ell j}^{(u,o)}, r, t) \, dt \right];$$

where the vector

$$\vec{\gamma} = [\gamma_{M11}, \ldots, \gamma_{M1N_1}, \ldots, \ldots, \gamma_{Mn1}, \ldots, \gamma_{MnN_n}], \tag{26}$$

contains all the undetermined coefficients γ_{Mji}, for $j = 1, \ldots, n$, being n total the number of ionic species, and $i = 1, \ldots, N_j$, being N_j the maximum number of nodes corresponding to the ionic species j.

We define the residual function for the species j as

$$\mathcal{R}_{Mj}(r; \vec{\gamma}) = \sum_{i=1}^{N_j} \gamma_{Mji} \, \phi_i(r) - \exp\left[-\beta U_{Mj}(r) + \widetilde{H}_{Mj}(r; \vec{\gamma}) - K_{Mj} \right], \tag{27}$$

which we would like to minimize. Thus, we apply the Collocation Method,[53]

$$\int_0^{t_{max}} \mathcal{R}_{Mj}(r; \vec{\gamma}) \, \delta(r - r_k) = \mathcal{R}_{Mj}(r_k; \vec{\gamma}) = 0, \tag{28}$$

where r_k corresponds to the position of the nodal point k.

As a result, Eq. (28) can be written as

$$\mathcal{R}_{Mj}(r_k; \vec{\gamma}) = \sum_{i=1}^{N_j} \gamma_{Mji} \, \phi_i(r_k)$$
$$- \exp\left[-\beta U_{Mj}(r_k) + \widetilde{H}_{Mj}(r_k; \vec{\gamma}) - K_{Mj} \right] = 0. \tag{29}$$

By using the following properties for the basis functions

$$\phi_i(r_k) = \delta_{ik}, \tag{30}$$

with δ_{ik} being the Kronecker delta, it is possible to write Eq. (29) as

$$\mathcal{R}_{Mj}(r_k; \vec{\gamma}) = \gamma_{Mjk} - \exp\left[-\beta U_{Mj}(r_k) + \widetilde{H}_{Mj}(r_k; \vec{\gamma}) - K_{Mj} \right] = 0, \tag{31}$$

which corresponds to a system of coupled non-linear integral equations. To use the Newton-Raphson method, we define

$$J\left(r; \vec{\gamma}^{[f]}\right) \left(\vec{\gamma}^{[f+1]} - \vec{\gamma}^{[f]}\right)^T = -\vec{\mathcal{R}}\left(r; \vec{\gamma}^{[f]}\right)^T, \tag{32}$$

where $J\left(r; \vec{\gamma}^{[f]}\right)$ is the Jacobian matrix, $\vec{\gamma}$ is a vector containing the real coefficients γ_{Mjk}, and $\vec{\mathcal{R}}\left(\vec{\gamma}^{[f]}\right)$ is a residual vector defined as

$$\vec{\mathcal{R}}\left(\vec{\gamma}^{[f]}\right) = \left[\mathcal{R}_{M1}^{[f]}(r_1), \ldots, \mathcal{R}_{M1}^{[f]}(r_{N_1}), \ldots, \ldots, \right.$$
$$\left. \mathcal{R}_{Mn}^{[f]}(r_1), \ldots, \mathcal{R}_{Mn}^{[f]}(r_{N_n}) \right], \tag{33}$$

where the superindex [f] indicates the current iteration number, and the superindex T indicates the transpose operation over the vector to

which it has been applied. The Jacobian matrix $J\left(\vec{\gamma}^{[f]}\right)$ is defined by the partial derivatives of the residual functions as follows:

$$
J\left(\vec{\gamma}^{[f]}\right) =
\begin{bmatrix}
\dfrac{\partial \mathcal{R}_{M1}^{[f]}(r_1)}{\partial \gamma_{M11}} & \cdots & \dfrac{\partial \mathcal{R}_{M1}^{[f]}(r_1)}{\partial \gamma_{M1N_1}} & \dfrac{\partial \mathcal{R}_{M1}^{[f]}(r_1)}{\partial \gamma_{Mn1}} & \cdots & \dfrac{\partial \mathcal{R}_{M1}^{[f]}(r_1)}{\partial \gamma_{MnN_n}} \\
\vdots & \ddots & \vdots & \vdots & \ddots & \vdots \\
\dfrac{\partial \mathcal{R}_{M1}^{[f]}(r_{N_1})}{\partial \gamma_{M11}} & \cdots & \dfrac{\partial \mathcal{R}_{M1}^{[f]}(r_{N_1})}{\partial \gamma_{M1N_1}} & \dfrac{\partial \mathcal{R}_{M1}^{[f]}(r_{N_1})}{\partial \gamma_{Mn1}} & \cdots & \dfrac{\partial \mathcal{R}_{M1}^{[f]}(r_{N_1})}{\partial \gamma_{MnN_n}} \\
\vdots & & \vdots & \vdots & & \vdots \\
\dfrac{\partial \mathcal{R}_{Mn}^{[f]}(r_1)}{\partial \gamma_{M11}} & \cdots & \dfrac{\partial \mathcal{R}_{Mn}^{[f]}(r_1)}{\partial \gamma_{M1N_1}} & \dfrac{\partial \mathcal{R}_{Mn}^{[f]}(r_1)}{\partial \gamma_{Mn1}} & \cdots & \dfrac{\partial \mathcal{R}_{Mn}^{[f]}(r_1)}{\partial \gamma_{MnN_n}} \\
\vdots & \ddots & \vdots & \vdots & \ddots & \vdots \\
\dfrac{\partial \mathcal{R}_{Mn}^{[f]}(r_{N_n})}{\partial \gamma_{M11}} & \cdots & \dfrac{\partial \mathcal{R}_{Mn}^{[f]}(r_{N_n})}{\partial \gamma_{M1N_1}} & \dfrac{\partial \mathcal{R}_{Mn}^{[f]}(r_{N_n})}{\partial \gamma_{Mn1}} & \cdots & \dfrac{\partial \mathcal{R}_{Mn}^{[f]}(r_{N_n})}{\partial \gamma_{MnN_n}}
\end{bmatrix}
\tag{34}
$$

where

$$
\mathcal{R}_{Mj}^{[f]}(r_k) = \mathcal{R}_{Mj}(r_k; \vec{\gamma}^{[f]}) = \gamma_{Mjk}^{[f]} - \exp\left[-\beta U_{Mj}(r_k) + \widetilde{H}_{Mj}^{[f]}(r_k) - K_{Mj}\right],
\tag{35}
$$

and

$$
\begin{aligned}
\widetilde{H}_{Mj}^{[f]}(r_k) &= \widetilde{H}_{Mj}(r_k; \vec{\gamma}^{[f]}) \\
&= \sum_{\ell=1}^{n} \sum_{u=1}^{3} \sum_{o=1}^{u} \sum_{m \in \{A,B\}} \sum_{v=1}^{5} \rho_\ell^{bulk} \\
&\quad \int_{P_{\ell j}^{*(u,m)}}^{\mathbb{Q}_{\ell j}^{*(u,m)}} \left[\left(\sum_{d=1}^{N_\ell} \gamma_{M\ell d}^{[f]} \phi_d(t) \right) \times \right. \\
&\quad \left. \vartheta_{\ell j}(o,v)\, \mathcal{J}\!\left(v, \check{\Lambda}_{\ell j}^{(u,o)}, \hat{\Lambda}_{\ell j}^{(u,o)}, r_k, t\right) dt \right].
\end{aligned}
\tag{36}
$$

Note that the partial derivatives $\dfrac{\partial \mathcal{R}_{Mj}^{[f]}(r_k)}{\partial \gamma_{Mab}}$ appearing in the Jacobian matrix can be calculated analytically

$$
\begin{aligned}
\frac{\partial \mathcal{R}_{Mj}^{[f]}(r_k)}{\partial \gamma_{Mab}} &= \delta_{(Mjk,\,Mab)} - \exp\left[-\beta U_{Mj}(r_k) \right. \\
&\quad \left. + \widetilde{H}_{Mj}^{[f]}(r_k) - K_{Mj} \right] \frac{\partial \widetilde{H}_{Mj}^{[f]}(r_k)}{\partial \gamma_{Mab}},
\end{aligned}
\tag{37}
$$

$$
= \delta_{(Mjk,\,Mab)} + \left[\mathcal{R}_{Mj}^{[f]}(r_k) - \gamma_{Mjk}^{[f]} \right] \frac{\partial \widetilde{H}_{Mj}^{[f]}(r_k)}{\partial \gamma_{Mab}},
\tag{38}
$$

where

$$
\begin{aligned}
\frac{\partial \widetilde{H}_{Mj}^{[f]}(r_k)}{\partial \gamma_{Mab}} &= \sum_{u=1}^{3} \sum_{o=1}^{u} \sum_{m \in \{A,B\}} \sum_{v=1}^{5} \rho_a^{bulk} \int_{P_{\ell j}^{*(u,m)}}^{\mathbb{Q}_{\ell j}^{*(u,m)}} \phi_b(t) \\
&\quad \left[\vartheta_{aj}^{(o,v)}\, \mathcal{J}\!\left(v, \check{\Lambda}_{aj}^{(u,o)}, \hat{\Lambda}_{aj}^{(u,o)}, r_k, t\right) dt \right].
\end{aligned}
\tag{39}
$$

Once we start from an initial guess [that can be as simple as $g_{Mj}(r) = 1$], the Newton-Raphson method allows us to generate a new solution whose convergence is quadratic if the candidate solution is close to the solution of Eq. (31). To determine whether

a numerical solution has been achieved, we monitor both the difference of the Euclidean norm between two successive solutions,

$$
\left\| \vec{\gamma}^{[f+1]} - \vec{\gamma}^{[f]} \right\|_2 = \left(\sum_{j=1}^{n} \sum_{k=1}^{N_j} \left| \gamma_{Mjk}^{[f+1]} - \gamma_{Mjk}^{[f]} \right|^2 \right)^{1/2},
\tag{40}
$$

and the global electroneutrality. On the other hand, the surface charge density over the macroion's surface can be calculated in terms of the radial distribution functions of all ionic species as

$$
\sigma_0^{sphere}(g_{M\ell}(t)) = -4\,e_0 \sum_{\ell=1}^{n} z_\ell \rho_\ell^{bulk} \int_{R_{M\ell}}^{\infty} \frac{t^2}{R_M^2}\, g_{M\ell}(t)\, dt.
\tag{41}
$$

If σ_0^{sphere} is the desired surface charge density over the macroion's surface, for non-zero valences of the central macroion, it is possible to define the relative error,

$$
E_r = \frac{\left| \sigma_0^{sphere} - \sigma_0^{sphere}(g_{M\ell}(t)) \right|}{\sigma_0^{sphere}}.
\tag{42}
$$

If the valence of the macroion is zero, it is possible to define the absolute error,

$$
E_a = \left| \sigma_0^{sphere} - \sigma_0^{sphere}(g_{M\ell}(t)) \right|.
\tag{43}
$$

Typically, we demand that $\left\| \vec{\gamma}^{[f+1]} - \vec{\gamma}^{[f]} \right\|_2 < 10^{-8}$ and $E_r < 10^{-8}$. The consideration of E_r and E_a, along with the Euclidean norm, allows a more robust and precise implementation of our finite element algorithm.

Once the radial distribution functions for all ionic species are known, it is possible to calculate the electrostatic properties of the electrical double layer in spherical geometry such as the integrated charge, the electric field, the mean electrostatic potential, and the capacitive compactness around a particle of species i, valence z_i, and diameter R_i as[26,54–56]

$$
P_i(r) = z_i + 4\pi \sum_{\ell=1}^{n} z_\ell \rho_\ell^{bulk} \int_0^r g_{i\ell}(t)\, t^2 dt,
\tag{44}
$$

$$
E_i(r) = \frac{e_0}{4\pi \varepsilon_0 \varepsilon_r} \frac{P_i(r)}{r^2},
\tag{45}
$$

$$
\begin{aligned}
\psi_i(r) &= \int_r^\infty E_i(t)\, dt = \frac{1}{\varepsilon_0 \varepsilon_r} \sum_{\ell=1}^{n} e_0\, z_\ell \rho_\ell^{bulk} \\
&\quad \times \int_{R_{i\ell}}^\infty g_{i\ell}(t)\, \frac{t}{r} \left(\frac{r - t - |r - t|}{2} \right) dt
\end{aligned}
\tag{46}
$$

and

$$
\tau_c^i = \left(\frac{2}{R_i} - 4\pi \varepsilon_0 \varepsilon_r \frac{\psi_i(r = R_i/2)}{z_i e_0} \right).
\tag{47}
$$

In general, note that by considering the global electroneutrality of an electrode–electrolyte system, it is possible to replace the real system with an effective capacitor, in which the diffuse electrical double-layer charge is placed in an electrode with a charge

equal in magnitude to that of the real solid electrode but with an opposite sign. The distance from the coordinate origin at which this electrode is located is precisely the capacitive compactness.[26,54–56] Notice that, if the location of the electrical double-layer electrode is measured from the surface of the real solid electrode, then the capacitive compactness can be also interpreted as the separation distance between both electrodes. In the literature, it is very well known that the Debye length, and the associated electrical double layer, shrinks as a function of the ionic strength of the supporting electrolyte. However, the Debye length cannot take into account the influence of the surface charge density of the electrode, as well as other relevant properties of Coulombic fluids such as ion correlations, ionic excluded volume effects, polarization effects, ionic-specific adsorption, etc. In this sense, the capacitive compactness is a generalization of the Debye length that has proven to be very useful to quantify the thickness or spatial extent of the ionic cloud neutralizing a charged surface.

To recover the point–ions limit from the HNC/MSA theory, we can consider that the diameters of all species are the same and equal to zero in the definition of the MSA direct correlation function, that is $R_\ell = R = 0$ for $\ell = 1, \ldots, n$. As a result, it is possible to write

$$c_{\ell j}^{\mathrm{MSA}}(s) = -z_\ell z_j \lambda_B\, s^{-1} \quad \text{for } s > 0, \tag{48}$$

given that $R_{\ell j} = \lambda_{\ell j} = 0$, where $\lambda_B = \beta e_0^2/(4\pi\varepsilon_0\varepsilon_r)$ is the Bjerrum length. On the other hand, the point–ions limit of the functions $H_{Mj}(r)$ and $K_{Mj}(r)$ can be written as

$$
\begin{aligned}
H_{Mj}^{R=0}(r) &= \lim_{\substack{R_\ell = 0 \\ \forall\, \ell}} H_{Mj}(r) \\
&= \sum_{\ell=1}^{n} \rho_\ell^{bulk} \int_{R_{M\ell}}^{t_{\max}} g_{M\ell}(t)\left[-z_\ell z_j \lambda_B\right] \frac{2\pi t}{r}(r + t - |r - t|)\, dt,
\end{aligned}
\tag{49}
$$

$$\lim_{\substack{R_\ell = 0 \\ \forall\, \ell}} K_{Mj} = -2\pi z_j \lambda_B \left(t_{max}\right)^2 \sum_{\ell=1}^{n} z_\ell\, \rho_\ell^{bulk} = 0, \tag{50}$$

where $t_{\max}$ is the upper limit of the integral corresponding to Eq. (49) when it goes to infinity and Eq. (50) is equal to zero due to the electroneutrality condition. Note that in Eq. (49), the inferior limit of the integral corresponds to the closest approach distance $R_{M\ell}$ between an ion of species ℓ and the central macroion. This means that the point ions do have an "ionic size" (i.e., a Stern correction) regarding the surface of the central macroion.

The electrostatic energy between the central macroion M and an ion of species j in terms of the ionic radial distribution functions can be expressed as

$$-\beta\, U_{Mj}(r) = -2\pi z_j \lambda_B \sum_{\ell=1}^{n} z_\ell\, \rho_\ell^{bulk} \int_{R_{M\ell}}^{t_{\max}} g_{M\ell}(t)\, \frac{t}{r}(-2\,t)\, dt. \tag{51}$$

By substituting Eqs. (49)–(51) in Eq. (5), it is possible to obtain

$$g_{Mj}(r) = \exp\left[-4\pi z_j \lambda_B \sum_{\ell=1}^{n} z_\ell\, \rho_\ell^{bulk} \int_{r}^{t_{\max}} g_{M\ell}(t)\left(t - \frac{t^2}{r}\right) dt\right], \tag{52}$$

or

$$g_{Mj}(r) = \exp\left[-\beta W_{Mj}(r)\right] = \exp\left[-z_j e_0 \beta\, \psi_M(r)\right]. \tag{53}$$

In Eq. (53), the potential of mean force $W_{Mj}(r)$ is equal to the electrostatic energy [see Eq. (46)] that an ion of species j feels at a distance r from the center of the central macroion, which corresponds to the non-linear Poisson–Boltzmann theory for n species, with different closest approach distances between the ions and the central macroion.

V. RESULTS AND DISCUSSION

With the aim of testing the theoretical approach proposed in this work, we have compared the theoretical and simulation colloid–colloid or colloid–ion radial distribution functions of positively and negatively charged colloids in different mixtures containing four or six species, either in the absence (SF case) or in the presence (AS case) of added salts. The corresponding SF and AS systems are described in Tables II and III. Given that the supporting electrolyte is composed of monovalent ions, it is expected that ion correlations should not play a major role. However, we foresee that excluded volume effects due to the finite size of colloids and/or small ions cannot be discarded, despite the large 1:333 size asymmetry considered here. Thus, the radial distribution functions of neutral colloids in the presence of a binary monovalent salt (SF–N case) and in the presence of a binary mixture of equally sized repulsive-core spheres (4S-RCS case), at the same concentration, are compared in Fig. 3 (the definition of the SF-N and the 4S-RCS systems is given in Tables II and III). In Fig. 3(a), it is observed that the colloid–colloid radial distribution functions associated with the SF-N and 4S-RCS systems are practically identical
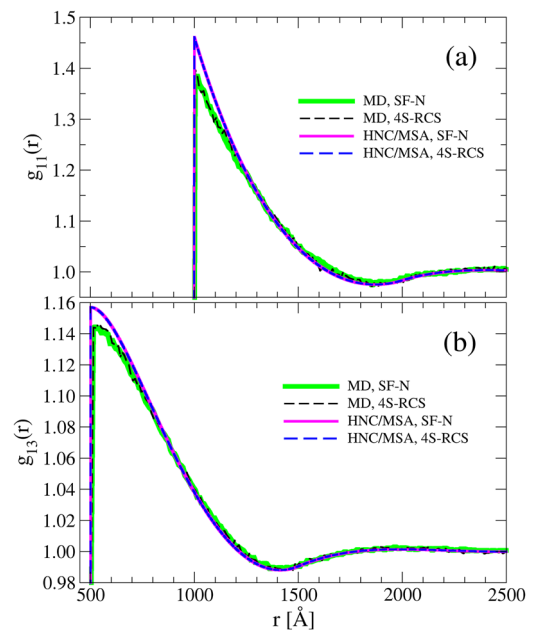
FIG. 3. Colloid–colloid and colloid–ion radial distribution functions for the salt-free (SF) and the salt-free with neutral colloids (SF–N) systems (described in Tables II and III). The radial distribution functions were obtained either via molecular dynamics (MD) simulations or via the HNC/MSA integral equations formalism proposed in this work. (a) $g_{11}(r)$ and (b) $g_{13}(r)$.

according to MD simulations. The same behavior is displayed by the analogous HNC/MSA curves, although they overestimate the contact values predicted by the simulation results. A colloid–colloid contact value larger than 1 is expected due to the volume fraction of the SF-N and 4S-RCS systems, namely, 0.1261245 in both instances. In addition, in Fig. 3(b), the colloid–ion radial distribution functions for the SF-N and 4S-RCS systems are shown. The same trends observed in Fig. 3(a) for the colloid–colloid radial distribution functions are observed here: colloid–ion contact values larger than 1, a non-monotonic behavior of the radial distribution functions, almost identical small particle profiles associated with the SF-N and 4S-RCS systems obtained either using MD simulations or the HNC/MSA theory, and HNC/MSA colloid–ion contact values that are slightly higher than those predicted by MD simulations. Thus, we conclude that ion correlations are certainly negligible in the SF-N system, where neutral colloids are dissolved in a monovalent supporting electrolyte. Moreover, the previous observations demonstrate that the colloid–colloid and colloid–ion contact values larger than 1, as well as the non-monotonic behavior of the corresponding radial distributions, are due essentially to entropic or excluded volume effects. This last ingredient is not taken into account in the classical non-linear Poisson–Boltzmann theory (NLPB). In fact, the numerical solution of the NLPB theory using our finite element approach for the SF-N system predicts a $g_{ij}(r) = 1$ for the colloid–colloid and colloid–ion radial distributions at distances larger than the closest ionic approach distance for each ionic species (not shown). As a result, important deviations from the NLPB theory are expected in the presence of charged colloids. Notice that for the SF-N, the interaction between the large neutral colloids and the small cations or small anions is the same by symmetry. Thus, the $g_{13}(r)$, $g_{14}(r)$, $g_{23}(r)$, and $g_{24}(r)$ are identical among them, and a charge density per unit volume equal to zero in the whole space is predicted consistently by MD simulations, the HNC/MSA theory, and the NLPB equation.

To study the effects of the colloidal charge on the colloid–colloid interaction in a mixture of positive and negative colloids, a comparison between the corresponding radial distribution functions has been performed for the salt-free (SF) and the added salt (AS) systems (defined in Tables II and III) in Figs. 4(a) and 4(b), respectively. In both figures, it is observed that the HNC/MSA radial distribution functions of equally, $g_{11}(r)$, and oppositely, $g_{12}(r)$, charged colloids are not monotonic and agree well with the radial distribution functions predicted by MD simulations. Moreover, MD simulations predict that the contact value of oppositely charged colloids, $g_{12}(r = 1000$ Å$)$, decreases when the
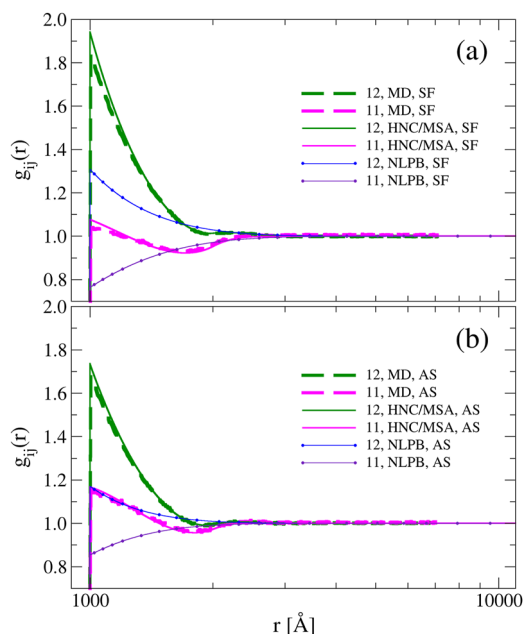
FIG. 4. Radial distribution functions between colloidal particles according to molecular dynamics (MD) simulations, HNC/MSA integral equations theory, and the non-linear Poisson–Boltzmann (NLPB) equation. (a) Salt-free (SF) system and (b) added salt (AS) system. The SF and AS systems are described in Tables II and III.

added salt concentration increases, as shown in Figs. 4(a) and 4(b) for the SF and the AS systems, respectively. When the added salt concentration increases, the ionic strength augments and the supporting 1 : 1 electrolyte promotes an enhanced colloidal charge neutralization. As a result, the electrostatic screening and the ionic excluded volume effects yielded by the added salt decrease the net electrostatic interaction between charged colloids. This is consistent with the increase in the contact value of equally charged colloids, $g_{11}(r = 1000$ Å$)$, when the AS system displayed in Fig. 4(b) is compared regarding the SF system portrayed in Fig. 4(a). On the other hand, the radial distribution functions predicted by the mean-field non-linear Poisson–Boltzmann (NLPB) theory are monotonic in the whole space and differ significantly from those obtained via MD simulations and the HNC/MSA integral equations theory. Despite these limitations, it is seen that the NLPB contact values of equally, $g_{11}(r = 1000$ Å$)$, and opposite, $g_{12}(r = 1000$ Å$)$, charged colloids

TABLE IV. Parameters of the added salt systems AS-S1, AS-S2, and AS-S2-N are described theoretically using the HNC/MSA formalism proposed in this work. The diameters of all particle species correspond to those used in the added salt (AS) system defined in Table II. By electroneutrality, $c_2 = c_1$, $c_4 = c_3$, and $c_6 = c_5$. The temperature and the dielectric constant, ε_r, in the whole space are 298 K and 78.5, respectively. Note that the added salt concentration in the AS-S1 is 500 times the concentration of colloids, whereas the added salt concentration in the AS-S2 and AS-S3 is 1000 times the concentration of colloids. Moreover, notice that the AS-S2 and AS-S2-N systems have the same volume fraction because they only differ in the valence of colloids. $\kappa_D = 1/\lambda_D$, where λ_D is the Debye length of the corresponding system.[1–3]

Case	z_1	z_2	z_3	z_4	z_5	z_6	$c_1(M)$	$c_3(M)$	$c_5(M)$	κ_D (Å^{-1})	λ_D (Å)	Vol. frac.
AS-S1	10	−10	−1	1	−1	1	2×10^{-7}	2×10^{-6}	1×10^{-4}	3.63×10^{-3}	275.35	0.126 132 4
AS-S2	10	−10	−1	1	−1	1	2×10^{-7}	2×10^{-6}	2×10^{-4}	4.90×10^{-3}	204.12	0.126 140 3
AS-S2-N	0	0	−1	1	−1	1	2×10^{-7}	2×10^{-6}	2×10^{-4}	4.67×10^{-3}	213.98	0.126 140 3
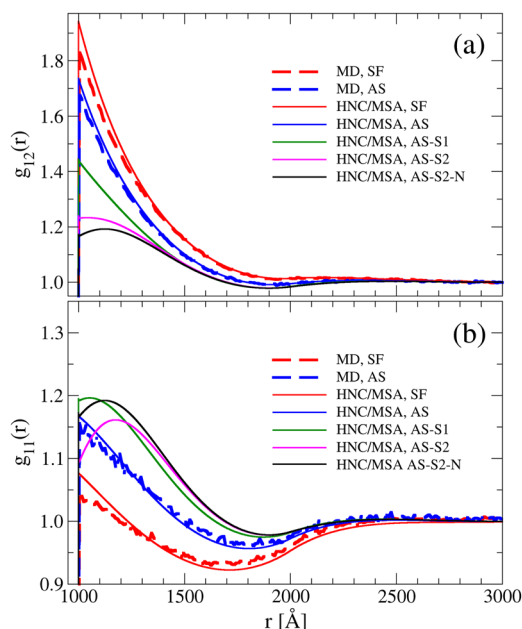
FIG. 5. Radial distribution function between colloidal particles for different added salt concentrations according to molecular dynamics (MD) simulations and the HNC/MSA integral equations theory. (a) $g_{12}(r)$ and (b) $g_{11}(r)$. The SF, AS, AS-S1, AS-S2, and AS-S2-N systems are described in Tables II–IV.

display the same trend predicted by MD simulations when the SF curves in Fig. 4(a) are contrasted with the corresponding ones in Fig. 4(b).

To test the influence of the ionic strength in the microscopic structure of the electrical double layer of a mixture of positive and negative colloids (see Table IV), in Fig. 5, it is shown the behavior of the colloid–colloid radial distribution functions $g_{12}(r)$ and $g_{11}(r)$, according to the HNC/MSA theory proposed in this work, when the concentration of the added salt increases in the AS system as shown in Table IV. In the case of oppositely charged colloids, it is observed that the contact value $g_{12}(r = 1000$ Å$)$ decreases monotonically when the ionic strength increases (compare systems SF, AS, AS-S1, and AS-S2). Moreover, the $g_{12}(r = 1000$ Å$)$ in the AS-S2 system seems to approach to the $g_{12}(r = 1000$ Å$)$ associated with the AS-S2-N system. The systems AS-S2 and AS-S2-N are identical except in the valence of the colloids, which is zero in the AS-S2-N system (neutral colloids), as shown in Table IV. On the other hand, in the case of equally charged colloids, the contact value $g_{11}(r = 1000$ Å$)$ increases when the ionic strength increases (compare systems SF, AS, and AS-S1). However, if the ionic strength is further increased, the contact value $g_{11}(r = 1000$ Å$)$ now decreases (compare the values associated with those of the AS-S2 and AS-S1). If the charge of colloids in the AS-S2 system vanishes, maintaining the same properties of the electrolyte (AS-S2-N system), the corresponding radial distribution function resembles that associated with the AS-S2 system, in which colloidal particles are highly screened electrostatically. To confirm the non-monotonic behavior of the contact value of

equally charged colloids predicted by the HNC/MSA in a mixture of positively and negatively charged colloids, it would be necessary to perform MD simulations of the systems AS-S2 and AS-S2-N considering 267 280 particles, which is ten times the number of particles simulated in the AS system (26 728) in this work. Such simulations would require also a very large number of time steps because the radial distribution functions of colloidal particles that are either uncharged or very strongly screened are usually very noisy. At this point, it is worth mentioning that the HNC/MSA formalism is a well-established liquid state theory, whose origins can be traced back to classical density functional theory.[31] In addition, the HNC/MSA theory has shown a good agreement regarding simulation results in a wide variety of systems in the past, see, e.g., Refs. 4, 27, 32, 45, 54, and 57–60. Thus, the confirmation of the behavior predicted by the HNC/MSA theory for the AS-S2 and the AS-S2-N systems is a rather stringent test of the predictive capacity of the theoretical formulation proposed in this work. In any case, we hope this theoretical prediction could be tested in the future by either other theoretical approaches[28,29] or by very long runs of large-scale molecular simulations.

The radial distribution functions associated with different species of small particles around a colloidal particle of species 1 for the salt-free (SF) and added salt (AS) systems are displayed
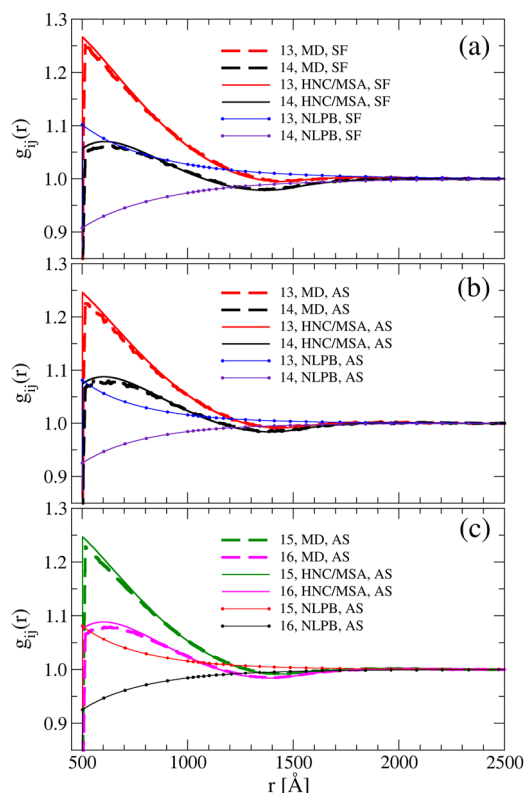
FIG. 6. Colloid–ion radial distribution functions according to molecular dynamics (MD) simulations, HNC/MSA integral equations theory, and the non-linear Poisson–Boltzmann (NLPB) equation. (a) Salt-free (SF) system, (b) and (c) added salt (AS) system. The SF and the AS systems are described in Tables II and III.
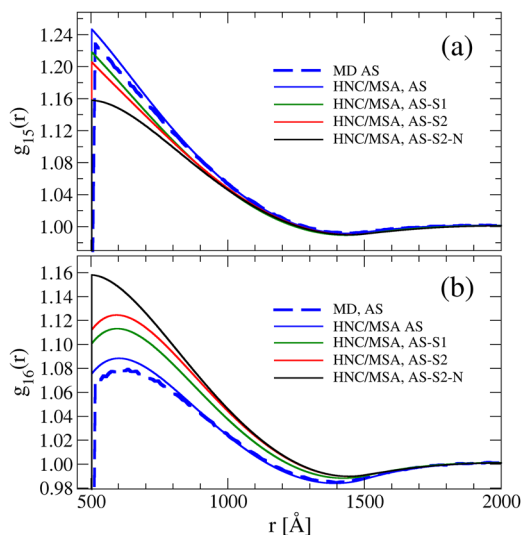
FIG. 7. Colloid–ion radial distribution functions for different added salt concentrations according to molecular dynamics (MD) simulations and HNC/MSA integral equations theory. (a) $g_{15}(r)$ and (b) $g_{16}(r)$. The SF, AS, AS-S1, AS-S2, and AS-S2-N systems are described in Tables II–IV.

in Fig. 6 (notice that by symmetry, identical profiles are observed if the central colloidal particle is of species 2). In all instances, the ionic profiles associated with the HNC/MSA integral equation theory display a non-monotonic behavior as a function of the
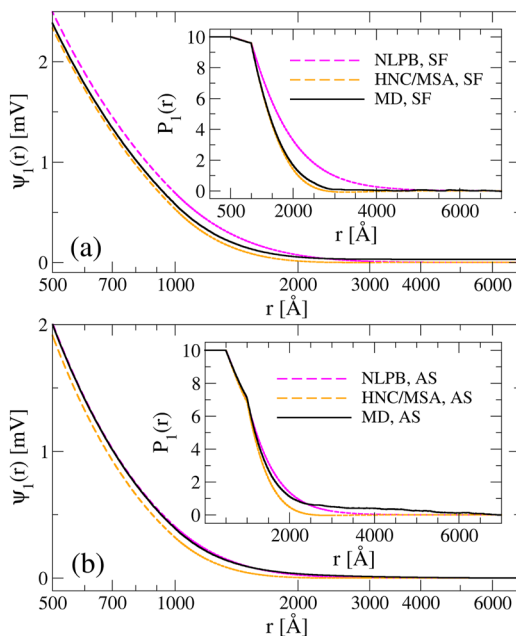
distance to the colloidal surface and compare well with the corresponding MD simulation curves, whereas the NLPB ionic profiles differ significantly from the simulation data displaying a monotonic conduct as a function of the distance to the colloidal surface. The ionic contact values $g_{13}(r = 501.5 \text{ Å})$ and $g_{14}(r = 501.5 \text{ Å})$ exhibit the same trends observed in the corresponding colloidal cases portrayed in Fig. 4 where the SF and AS cases have been compared. On the other hand, in the AS case, it is observed that the ionic profiles associated with ions with 3 Å of diameter (that are counterions of the colloidal particles) and the ionic profiles of particles with 5 Å of diameter (that correspond to the added salt species) are very similar for ions with the same valence. Moreover, note that the curves associated with the AS ionic species with 5 Å of diameter are smoother than the curves associated with the SF ionic species with 3 Å of diameter. This is due to a large number of added salt ions present in the simulation box, in comparison to the number of small counterions in the SF case, as shown in Table III. In addition, the behavior of the colloid–ion radial distribution functions when the added salt concentration increases is displayed in Fig. 7. Here, it is observed that the contact values of the colloid–ion radial distribution functions g_{15} and g_{16} decrease and increase monotonically, respectively, when the salt (or the ionic strength) increases. Moreover, in both instances, they approach the small particle profiles of the AS-S2-N system. In this last system, the colloids are neutral, and the supporting electrolyte is identical to that present in the AS-S2 system, in which the colloids are charged but highly screened electrostatically due to the large concentration of the added salt.

In Fig. 8, the integrated charge, $P_1(r)$, and the mean electrostatic potential, $\psi_1(r)$, around a colloidal particle of species 1 are displayed. These quantities correspond to the SF and AS radial distribution functions displayed in Figs. 4 and 6. Here, it is observed that $P_1^{AS}(r) < P_1^{SF}(r)$ and $\psi_1^{AS}(r) < \psi_1^{SF}(r)$ close to the colloidal surface for simulations and theories, which is a consequence of the

FIG. 8. Mean electrostatic potential $\psi_1(r)$ (main figures) and integrated charge $P_1(r)$ (insets) around a colloidal particle of species 1. (a) Salt-free (SF) system and (b) added salt (AS) system. The SF and AS systems are described in Tables II and III.
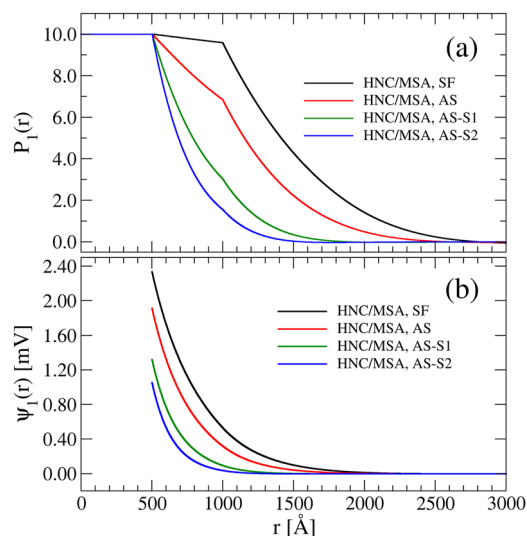
FIG. 9. (a) Mean electrostatic potential $\psi_1(r)$ and (b) integrated charge $P_1(r)$ around a colloidal particle of species 1 predicted by the HNC/MSA theory proposed in this work. The SF, AS, AS-S1, and AS-S2 systems are described in Tables II–IV.

additional electrostatic screening yielded by the added salt ions. Another very interesting behavior is the good agreement displayed by the NLPB regarding MD simulations at the level of the mean electrostatic potential, despite the significant differences shown by the corresponding radial distribution functions in Figs. 4 and 6. This striking feature might explain why the DLVO theory has been very successful to model the force and the potential of mean force between macroions in weakly charged colloidal solutions in the presence of monovalent salts.

The behavior of the integrated charge, $P(r)$, and the mean electrostatic potential, $\psi(r)$, as a function of the distance for several added salt concentrations, according to the HNC/MSA theory proposed in this work, are shown in Fig. 9. These quantities that correspond to the SF, AS, AS-S1, and AS-S2 radial distribution functions are displayed in Figs. 5 and 7. Here, it is observed that $P_1^b(r) < P_1^a(r)$ and $\psi_1^b(r) < \psi_1^a(r)$ if the added salt concentration in the system b is larger than the added salt concentration in the system a, that is if the ionic strength in the system b is larger regarding the system a. Moreover, the mean electrostatic potential and the integrated charge decrease monotonically as a function of the distance near the colloidal surface. Note that these electrostatic properties cannot be calculated by effective DLVO-like colloid-colloid interaction potentials.[1–3,34] This is perhaps one of the main advantages of the theoretical formalism proposed in the present work.

VI. CONCLUSIONS

A theoretical finite element description of the ionic profiles of a mixture of n species around a spherical macroion, with arbitrary size and charge asymmetries, has been proposed in this work. Ion correlations and ionic excluded volume effects are taken into account in the Ornstein–Zernike integral equations theory solved via the hybrid hypernetted chain/mean spherical approximation (HNC/MSA) closure. The classical non-linear Poisson–Boltzmann theory for n ionic species—with different ionic closest approach distances to the colloidal surface—is recovered from the HNC/MSA theory as a limit case. To illustrate the accuracy of this theoretical formulation, the electrical double layer of an electroneutral mixture of oppositely charged colloids and small ions, highly asymmetric in size and valence, has been studied in salt-free and added salt environments. Our theoretical formalism has displayed very good agreement regarding the ionic profiles obtained from molecular dynamics simulations with explicit small-sized ions. Interestingly, it has been observed that although the non-linear Poisson–Boltzmann colloid–colloid and colloid–ion profiles differ notably from those obtained via simulations with explicit ions, the associated mean electrostatic potential agrees well with the corresponding data associated with SF and AS simulations in the presence of explicit small–sized ions.

Regarding the parameter ranges in which the theoretical approaches used in this work should provide accurate results in comparison with primitive model simulations, we would like to mention that ion correlations and ionic excluded volume effects are not taken into account in the non-linear Poisson–Boltzmann equation. As a result, it is expected that the NLPB theory breaks down in the presence of colloidal particles at large volume fractions and/or high colloidal surface charge densities, far from the

ideal gas regime. Regarding the adequacy of HNC-based integral equations to describe the kind of Coulombic fluids considered here, we recall that the approximate closures involved in the HNC/MSA and HNC/HNC formalisms most likely result in some limitations of these theories. More specifically, in the case of HNC/HNC, it is well known the inexistence of numerical solutions for this integral equation in some regions of the parameter space of primitive model systems,[29,61] and besides, there is the occurrence of spurious peaks in the pair distribution function for ions of the same species.[62–64] On the other hand, the HNC/MSA formalism predicts an inaccurate potential–charge relationship for very highly charged electrical double layers ($\gtrsim 0.44$ C/m^2)[65] and, also, fails to exhibit a potential of zero charge in the case of double layers with valence-asymmetric restricted primitive model electrolytes.[26] At all events, the performance of any theoretical description of charged fluids must be evaluated case by case, and in particular, the diverse comparisons reported in this work evidence a very good concordance between the predictions of our new HNC/MSA account of a mixture of n ionic species with arbitrary size and charge asymmetries and the corresponding computer simulations. In addition, we would like to emphasize the notable power of the present treatment, since, in principle, it allows us to deal with systems composed of an *arbitrary* number of ionic species. Here, and just as an example, we have considered up to six species, but in practice, the limitations of our scheme are only those imposed by the capabilities of the hardware employed.

The theoretical radial distribution functions obtained from this general HNC/MSA framework could be used as an input for sophisticated electrophoresis theories in which hydrodynamic and ionic relaxation effects are taken into account.[66–69]

Another interesting extension of the present work is the possibility of obtaining the explicit generalization of the HNC/MSA theory for n species, with arbitrary asymmetry in size and valence, in planar geometry. This could be achieved by inflating the central macroion to reach the planar limit when the macroion radius goes to infinity. To our best knowledge, this formulation has not been reported in the literature using the HNC/MSA hybrid closure. Such a framework could be very useful to model, for instance, charged membranes, lipid bilayers, or electrical double-layer supercapacitors or batteries in the presence of Coulombic fluids.[5,20–22,24,30,70–72] Work along this line is currently in progress, and it will be published soon elsewhere.

SUPPLEMENTARY MATERIAL

The behavior of the repulsive-core and bare Coulomb potentials used in the molecular dynamics simulations presented in this study are portrayed in the supplementary material document (as a function of the distance) for typical colloid-colloid, colloid-ion, and ion-ion pair interaction potentials. In addition, in order to corroborate that the theory presented in this paper was correctly implemented, we have compared the results produced by our computational finite element implementation with previous HNC/MSA published data for two systems: one constituted by size-asymmetric ions around a central macroion,[4] and another one containing identical macroions at finite concentration in the presence of equally sized small ions at a volume fraction 0.24.[32]

AUTHOR DECLARATIONS

Conflict of Interest

The authors have no conflicts to disclose.

Author Contributions

Jonathan Josué Elisea-Espinoza: Data curation (lead); Investigation (lead); Methodology (lead); Validation (lead). **Enrique González-Tovar**: Supervision (lead); Writing – review & editing (lead). **Guillermo Iván Guerrero-García**: Conceptualization (lead); Formal analysis (lead); Writing – original draft (lead).

DATA AVAILABILITY

The data that support the findings of this study are available from the corresponding author upon reasonable request.

APPENDIX A: THE MSA DIRECT CORRELATION FUNCTIONS

If the average of the sum and difference of the ionic diameters of species i and j are defined as $R_{ij} = (R_j + R_i)/2$ and $\lambda_{ij} = (R_j - R_i)/2$, respectively, and considering that $R_i \leq R_j$, the MSA direct correlation functions can be written, in terms of $s = |\vec{r} - \vec{t}| = \sqrt{r^2 + t^2 - 2rt \cos \theta}$, as the sum of an electrostatic and a hard sphere contribution,[73–76]

$$c_{ij}^{MSA}(s) = c_{ij}^{hs}(s) + c_{ij}^{elec}(s), \tag{A1}$$

where

$$c_{ij}^{hs}(s) = \begin{cases} 0 & \text{if } R_{ij} \leq s, \\ -p_{ij}s^{-1} - q_{ij} - v_{ij}s - ws^3 & \text{if } \lambda_{ij} \leq s < R_{ij}, \\ -q_i & \text{if } 0 \leq s < \lambda_{ij}, \end{cases} \tag{A2}$$

with

$$p_{ij} = -\frac{\lambda_{ij}^2}{2}(A + 2BR_{ij} + CR_{ij}^2), \tag{A3}$$

$$q_{ij} = \frac{q_i + q_j}{2}, \tag{A4}$$

$$v_{ij} = \frac{v_i + v_j}{2}, \tag{A5}$$

$$q_i = \frac{1}{1 - \Upsilon_3} + AR_i + BR_i^2 + \frac{1}{3}CR_i^3, \tag{A6}$$

$$v_i = -\frac{1}{2}(A + 2BR_i + CR_i^2), \tag{A7}$$

$$w = \frac{1}{2}\sum_k^n \eta_k q_k, \tag{A8}$$

$$A = 3\frac{\Upsilon_2}{(1 - \Upsilon_3)^2}, \tag{A9}$$

$$B = 3\left[\frac{\Upsilon_1}{(1 - \Upsilon_3)^2} + \frac{3\Upsilon_2^2}{(1 - \Upsilon_3)^3}\right], \tag{A10}$$

$$C = 3\left[\frac{\Upsilon_0}{(1 - \Upsilon_3)^2} + \frac{6\Upsilon_1\Upsilon_2}{(1 - \Upsilon_3)^3} + \frac{9\Upsilon_2^3}{(1 - \Upsilon_3)^4}\right], \tag{A11}$$

$$\Upsilon_m = \sum_k^n \eta_k R_k^m, \tag{A12}$$

$$\eta_k = \frac{\pi}{6}\rho_k^{bulk}, \tag{A13}$$

and

$$c_{ij}^{elec}(s) = \begin{cases} -z_i z_j \lambda_B s^{-1} & \text{if } R_{ij} \leq s, \\ \alpha_0 s^{-1} + \alpha_1 + \alpha_2 s + \alpha_3 s^3 & \text{if } \lambda_{ij} \leq s < R_{ij}, \\ \beta_0 & \text{if } 0 \leq s < \lambda_{ij}, \end{cases} \tag{A14}$$

where $\lambda_B = \beta e_0^2/(4\pi\varepsilon_0\varepsilon_r)$ is the Bjerrum length and

$$\omega = \frac{e_0^2\beta}{4\pi\varepsilon_r\varepsilon_0} \tag{A15}$$

$$\beta_0 = 2\omega\left[z_i N_i - X_i R_i \chi + \frac{R_i^3}{3}\chi^2\right], \tag{A16}$$

$$\alpha_0 = \omega\lambda_{ij}^2\left\{(X_i + X_j)\chi - \left[(R_{ij}\chi)^2 - N_i N_j\right]\right\}, \tag{A17}$$

$$\alpha_1 = \omega\left\{\frac{\chi^2}{3}\left[R_i^3 + R_j^3\right] - (X_i - X_j)(N_i - N_j) - (X_i^2 + X_j^2)\Gamma - 2R_{ij}N_i N_j\right\}, \tag{A18}$$

$$\alpha_2 = \omega\left\{(X_i + X_j)\chi + N_i N_j - \frac{\chi^2}{2}(R_i^2 + R_j^2)\right\}, \tag{A19}$$

$$\alpha_3 = \omega\frac{\chi^2}{3}, \tag{A20}$$

$$X_k = \frac{z_k + R_k^2\chi}{1 + \Gamma R_k}, \tag{A21}$$

$$N_k = \frac{R_k\chi - z_k\Gamma}{1 + \Gamma R_k}, \tag{A22}$$

$$\chi = \frac{-\varrho \sum_{k=1}^{n} \rho_k^{bulk} R_k z_k \left(1 + \Gamma R_k\right)^{-1}}{1 + \varrho \sum_{k=1}^{n} \rho_k^{bulk} R_k^3 \left(1 + \Gamma R_k\right)^{-1}} \qquad (A23)$$

$$\varrho = \frac{\pi}{2}\left[1 - \Upsilon_3\right]^{-1}; \qquad (A24)$$

$$c_{ij}^{\text{MSA}}(s) = \begin{cases} -z_i z_j \lambda_B \, s^{-1} & \text{if } R_{ij} \le s, \\ (\alpha_0 - p_{ij})s^{-1} + (\alpha_1 - q_{ij}) + (\alpha_2 - v_{ij})s + (\alpha_3 - w)s^3 & \text{if } \lambda_{ij} \le s < R_{ij}, \\ \beta_0 - q_i & \text{if } 0 \le s < \lambda_{ij}. \end{cases} \qquad (A26)$$

Please note that in the definition of the coefficients q_i and β_0 [Eqs. (A6) and (A16), respectively], the subscript i indicates that we are considering the smallest particle species between i and j, which in this case is i, given that we are considering here that $R_i \le R_j$.

APPENDIX B: DEFINITION OF THE $\vartheta_{\ell j}$ MATRIX

Considering that $R_\ell \le R_j$, the direct correlation function defined in Eq. (A26) can be equivalently written as

$$c_{\ell j}^{\text{MSA}}(s) = \begin{cases} -z_\ell z_j \lambda_B \, s^{-1} & \text{if } s \in \mathbb{Z}_{\ell j}^1(s) \\ (\alpha_0 - p_{\ell j})s^{-1} + (\alpha_1 - q_{\ell j}) + (\alpha_2 - v_{\ell j})s + (\alpha_3 - w)s^3 & \text{if } s \in \mathbb{Z}_{\ell j}^2(s) \\ \beta_0 - q_\ell & \text{if } s \in \mathbb{Z}_{\ell j}^3(s) \end{cases} \qquad (B1)$$

where

$$\mathbb{Z}_{\ell j}^1(s) = \left\{ s = |\vec{r} - \vec{t}| \; : \; R_{\ell j} \le s < \infty \right\}$$
$$\mathbb{Z}_{\ell j}^2(s) = \left\{ s = |\vec{r} - \vec{t}| \; : \; \lambda_{\ell j} \le s < R_{\ell j} \right\}. \qquad (B2)$$
$$\mathbb{Z}_{\ell j}^3(s) = \left\{ s = |\vec{r} - \vec{t}| \; : \; 0 \le s < \lambda_{\ell j} \right\}$$

In order to ease the matrix formulation of the HNC/MSA theory, let us define the matrix of real coefficients,

$$\varpi_{\ell j} = \begin{bmatrix} -z_\ell z_j \lambda_B & 0 & 0 & 0 & 0 \\ (\alpha_0 - p_{\ell j}) & (\alpha_1 - q_{\ell j}) & (\alpha_2 - v_{\ell j}) & 0 & (\alpha_3 - w) \\ 0 & \beta_0 - q_\ell & 0 & 0 & 0 \end{bmatrix}; \qquad (B3)$$

where the parameter Γ is found by solving the following non-linear equation,

$$\Gamma^2 = \pi\omega D(\Gamma) = \pi\omega \sum_{k=1}^{n} \rho_k^{bulk} X_k^2. \qquad (A25)$$

Thus, the MSA direct correlation function can be written as

then $\vartheta_{\ell j}(u, v)$ can be defined as

$$\vartheta_{\ell j}(u, v) = \begin{cases} \varpi_{\ell j}^{(u=1, v)} \text{ if } \vec{t} = (t, \theta, \varphi) \in \mathbb{Z}_{\ell j}^1(s) \\ \varpi_{\ell j}^{(u=2, v)} \text{ if } \vec{t} = (t, \theta, \varphi) \in \mathbb{Z}_{\ell j}^2(s) \\ \varpi_{\ell j}^{(u=3, v)} \text{ if } \vec{t} = (t, \theta, \varphi) \in \mathbb{Z}_{\ell j}^3(s) \end{cases} \qquad (B4)$$

for $v = 1, \dots, 5$. In this formulation, the coefficients $\vartheta_{\ell j}(u, v)$ are real numbers that do not depend explicitly on s, even though the value of s in the three-dimensional space determines the value of the u, v component of the $\vartheta_{\ell j}$ matrix.

REFERENCES

[1] R. J. Hunter, *Zeta Potential in Colloid Science* (Academic Press, New York, 1981).
[2] R. J. Hunter, *Foundations of Colloid Science* (Clarendon, Oxford, 1987).
[3] W. B. Russell, D. A. Saville, and W. R. Schowalter, *Colloidal Dispersions* (Cambridge University Press, Cambridge, UK, 1989).
[4] G. I. Guerrero-García, E. González-Tovar, and M. Olvera de la Cruz, Soft Matter **6**, 2056 (2010).
[5] G. I. Guerrero-García, Biophys. Chem. **282**, 106747 (2022).
[6] G. I. Guerrero-García, J. Mol. Liq. **361**, 119566 (2022).
[7] M. Elimelech and C. R. O'Melia, Colloids Surf. **44**, 165–178 (1990).
[8] K. Besteman, M. A. G. Zevenbergen, H. A. Heering, and S. G. Lemay, Phys. Rev. Lett. **93**, 170802 (2004).
[9] F. H. J. van der Heyden, D. Stein, K. Besteman, S. G. Lemay, and C. Dekker, Phys. Rev. Lett. **96**, 224502 (2006).
[10] G. I. Guerrero-García, Y. Jing, and M. Olvera de la Cruz, Soft Matter **9**, 6046–6052 (2013).
[11] I. Semenov, S. Raafatnia, M. Sega, V. Lobaskin, C. Holm, and F. Kremer, Phys. Rev. E **87**, 022302 (2013).
[12] E.-Y. Kim and S.-C. Kim, J. Korean Phys. Soc. **68**, 658–667 (2016).
[13] S. Jang, G. R. Shin, and S.-C. Kim, Mol. Phys. **115**, 2411–2422 (2017).
[14] S. Jang, G. R. Shin, and S.-C. Kim, J. Mol. Liq. **237**, 282–288 (2017).
[15] S. Jang, G. R. Shin, and S.-C. Kim, J. Chem. Phys. **147**, 036101 (2017).
[16] S. Jang, G. R. Shin, and S.-C. Kim, J. Korean Phys. Soc. **73**, 1315–1323 (2017).
[17] E. Keshavarzi and M. Abareghi, J. Mol. Liq. **318**, 114271 (2020).
[18] E. Keshavarzi and M. Abareghi, J. Electroanal. Chem. **883**, 115060 (2021).

15 August 2023 14:56:31

[19] E. Keshavarzi, S. Rabiei-Jildani, and M. Abareghi, J. Appl. Electrochem. **51**, 1229–1240 (2021).

[20] S. Zhou, J. Phys. Chem. Solids **148**, 109705 (2022).

[21] S. Zhou, Nanomaterials **12**, 2534 (2022).

[22] S. Zhou and S. Lamperski, J. Phys. Chem. Solids **161**, 110440 (2022).

[23] S. Zhou and R. Zhou, Phys. Scr. **97**, 085402 (2022).

[24] S. Rabiei Jildani and E. Keshavarzi, Electrochim. Acta **426**, 140832 (2022).

[25] S. Yang, Y. Deng, and S. Zhou, Nanomaterials **13**, 16 (2023).

[26] G. I. Guerrero-García, L. B. Bhuiyan, C. W. Outhwaite, and E. González-Tovar, J. Mol. Liq. **367**, 120538 (2022).

[27] G. I. Guerrero-García, P. González-Mozuelos, and M. O. de la Cruz, J. Chem. Phys. **135**, 164705 (2011).

[28] M. Heinen, E. Allahyarov, and H. Löwen, J. Comput. Chem. **35**, 275 (2014).

[29] J. M. Falcón-González, C. Contreras-Aburto, M. Lara-Peña, M. Heinen, C. Avendaño, A. Gil-Villegas, and R. Castañeda-Priego, J. Chem. Phys. **153**, 234901 (2020).

[30] J.-P. Hansen and I. R. McDonald, *Theory of Simple Liquids* (Academic Press, London, 1986).

[31] S. L. Carnie, D. Y. C. Chan, D. J. Mitchell, and B. W. Ninham, J. Chem. Phys. **74**, 1472 (1981).

[32] A. González-Calderón, M. Chávez-Páez, E. González-Tovar, and M. Lozada-Cassou, J. Phys. Chem. B **122**, 7002 (2018).

[33] J. K. Chung and A. R. Denton, Phys. Rev. E **88**, 022306 (2013).

[34] N. Boon, G. I. Guerrero-García, R. van Roij, and M. Olvera de la Cruz, Proc. Natl. Acad. Sci. U. S. A. **112**, 9242 (2015).

[35] A. R. Denton, Phys. Rev. E **96**, 062610 (2017).

[36] B. M. Weight and A. R. Denton, J. Chem. Phys. **148**, 114904 (2018).

[37] G. J. Ojeda-Mendoza, A. Moncho-Jordá, P. González-Mozuelos, C. Haro-Pérez, and L. F. Rojas-Ochoa, Soft Matter **14**, 1355 (2018).

[38] E. Allahyarov, H. Löwen, and A. R. Denton, Phys. Chem. Chem. Phys. **24**, 15439 (2022).

[39] E. Allahyarov and H. Löwen, J. Chem. Phys. **157**, 164902 (2022).

[40] B. Beresford-Smith and D. Y. C. Chan, Chem. Phys. Lett. **92**, 474 (1982).

[41] V. Lobaskin and P. Linse, J. Chem. Phys. **109**, 3530 (1998).

[42] V. Lobaskin and P. Linse, Phys. Rev. Lett. **83**, 4208 (1999).

[43] P. Linse, J. Chem. Phys. **113**, 4359 (2000).

[44] J. Rydén, M. Ullner, and P. Linse, J. Chem. Phys. **123**, 034909 (2005).

[45] G. I. Guerrero-García, P. González-Mozuelos, and M. Olvera de la Cruz, ACS Nano **7**, 9714 (2013).

[46] J. D. Weeks, D. Chandler, and H. C. Andersen, J. Chem. Phys. **54**, 5237–5247 (1971).

[47] J. A. Anderson, J. Glaser, and S. C. Glotzer, Comput. Mater. Sci. **173**, 109363 (2020).

[48] D. N. LeBard, B. G. Levine, P. Mertmann, S. A. Barr, A. Jusufi, S. Sanders, M. L. Klein, and A. Z. Panagiotopoulos, Soft Matter **8**, 2385–2397 (2012).

[49] R. W. Hockney and J. W. Eastwood, *Computer Simulations Using Particles* (McGraw-Hill, New York, 1981).

[50] M. Deserno and C. Holm, J. Chem. Phys. **109**, 7694 (1998).

[51] E. A. Barrios-Contreras, E. González-Tovar, and G. I. Guerrero-García, Mol. Phys. **113**, 1190–1205 (2015).

[52] J. J. Elisea-Espinoza, E. González-Tovar, J. A. Martínez-González, C. G. Galván Peña, and G. I. Guerrero-García, Mol. Phys. **119**, e1916633 (2021).

[53] L. Mier y Teran, E. Díaz-herrera, M. Lozada-Cassou, and R. Saavedra-barrera, J. Comput. Phys. **84**, 326 (1989).

[54] G. I. Guerrero-García, E. González-Tovar, M. Chávez-Páez, J. Kłos, and S. Lamperski, Phys. Chem. Chem. Phys. **20**, 262–275 (2018).

[55] G. I. Guerrero-García, E. González-Tovar, M. Chávez-Páez, and T. Wei, J. Mol. Liq. **277**, 104–114 (2019).

[56] E. González-Tovar, J. A. Martínez-González, C. G. Galván Peña, and G. I. Guerrero-García, J. Chem. Phys. **154**, 096101 (2021).

[57] G. I. Guerrero-García, E. González-Tovar, M. Lozada-Cassou, and F. de J Guevara-Rodríguez, J. Chem. Phys. **123**, 034703 (2005).

[58] G. I. Guerrero-García, E. González-Tovar, and M. Chávez-Páez, Phys. Rev. E **80**, 021501 (2009).

[59] G. I. Guerrero-García, E. González-Tovar, and M. Olvera de la Cruz, J. Chem. Phys. **135**, 054701 (2011).

[60] G. I. Guerrero-García, E. González-Tovar, M. Quesada-Pérez, and A. Martín-Molina, Phys. Chem. Chem. Phys. **18**, 21852 (2016).

[61] L. Belloni, J. Chem. Phys. **98**, 8080 (1993).

[62] P. J. Rossky, J. B. Dudowicz, B. L. Tembe, and H. L. Friedman, J. Chem. Phys. **73**, 3372 (1980).

[63] D. Henderson, M. Lozada-Cassou, and L. Blum, J. Chem. Phys. **79**, 3055 (1983).

[64] F. O. Raineri and G. Stell, Condens. Matter Phys. **4**, 621 (2001).

[65] L. Mier-y-Teran, S. H. Suh, H. S. White, and H. T. Davis, J. Chem. Phys. **92**, 5087 (1990).

[66] M. Lozada-Cassou and E. González-Tovar, J. Colloid Interface Sci. **239**, 285 (2001).

[67] M. Lozada-Cassou, E. González-Tovar, and W. Olivares, Phys. Rev. E **60**, R17 (2001).

[68] C. Contreras Aburto and G. Nägele, J. Chem. Phys. **139**, 134109 (2013).

[69] C. C. Aburto and G. Nägele, J. Chem. Phys. **139**, 134110 (2013).

[70] A. K. Rakshit, B. Naskar, and S. P. Moulik, Colloids Surf., A **626**, 127084 (2021).

[71] X. Zhou, W.-B. Zhang, X.-W. Han, S.-S. Chai, S.-B. Guo, X.-L. Zhang, L. Zhang, X. Bao, Y.-W. Guo, and X.-J. Ma, ACS Appl. Energy Mater. **5**, 3979 (2022).

[72] A. J. Paulista Neto, D. A. C. da Silva, V. A. Gonçalves, H. Zanin, R. G. Freitas, and E. E. Fileti, Phys. Chem. Chem. Phys. **24**, 3280 (2022).

[73] K. Hiroike, J. Phys. Soc. Jpn. **27**, 1415 (1969).

[74] L. Blum, Mol. Phys. **30**, 1529 (1975).

[75] L. Blum and J. S. Hoeye, J. Phys. Chem. **81**, 1311 (1977).

[76] K. Hiroike, Mol. Phys. **33**, 1195 (1977).

15 August 2023 14:56:31